Absorbance and energy levels for a Fe^{3+} ion in α-Al_2O_3. Optical pumping applied to a 31 GHz Maser

M. Mrad,[1,*] A. Tarhini,[1,†] and Vincent Giordano[2,‡]

[1] *Department of Physics, Faculty of Sciences I & V, Lebanese University, Hadat and Nabatieh, Lebanon.*

[2] *Laboratoire FEMTO-ST, 26 Chemin de l'Epitaphe, 25000 Besanon, France.*

The structure of $3d^5$ configuration ion in a trigonal field is theoretically determined on the basis of a 252×252 matrix of complete energy. The spectra of paramagnetic electron resonance and the optical absorption of the Fe^{3+} ion in sapphire crystal ($\alpha - Al_2O_3$) have been calculated by diagonalizing the matrix of total energy. The obtained results are in good agreement with experimental observations. The strength of probability transitions between energy levels pairs are also established to show the possibility for achieving the inversion of the population in the fundamental state when applying the optical pumping mechanism to the crystal. The results based on the computed parameters of transition and on the maser effect equations show that a maser signal of a 31 GHz can be generated and that depends on the cryogenic design of the resonator.

Keywords: Energy-levels, Molecular Hamiltonian, Transition parameter, Absorbance, Shuffled complex evolution, Maser effect, State equations.

I. INTRODUCTION

Masers based on paramagnetic ions hosted in a crystal have been widely studied and used as stable microwave sources or as low noise amplifiers in the 60's [1]. The Maser action was obtained at low temperature in different doped crystals, the most popular of which was sapphire doped with Cr^{3+} or Rubis. Many types of maser have been designed generally from a doped crystal inserted in a waveguide or from a metal cavity cooled to the temperature of liquid helium. The doping level was typically around 0.05% and for an X-band source, the cryogenic resonator exhibited a Q-factor of the order of 10000 or less. Most systems were based on the multiplicity of ground state levels to obtain the population inversion required by the action of microwave pumping. Some attempts to optically pump the crystal has been made [2, 3]. But no real advantage over the classic Maser scheme has been demonstrated. The absence of a narrow band and an easy-to-handle laser source as well as the poor quality of the doped crystals available were certainly the main difficulties in obtaining a reliable optical pumped microwave maser. Finally, interest in this technology was almost stopped after the development of low noise cryogenic semiconductor amplifiers, stable quartz oscillators and low noise frequency synthesis.

More recently, we reported the possibility to get a 12 GHz maser signal presenting a short term relative frequency instability below 1×10^{-14} at short term with a large marge of progress [4, 5]. Such a frequency stability performance is required for a number of very demanding applications as metrology, space navigation, radio astronomy or fundamental physic experiments. The search for a reliable microwave source presenting a relative frequency stability of some 10^{-15} is a challenge that motivates a lot of innovative works all around the world [6–8]. In our first prototype the sustaining amplification is achieved in a cryogenic sapphire whispering gallery mode resonator containing a small amount of paramagnetic Fe^{3+} ions. The Fe^{3+} ion exhibits three ground state energy levels. A population inversion is obtained between the two lower ground state levels by submitting the Fe^{3+} ions to a 31 GHz signal. The maser oscillation takes place at 12.04 GHz. As the sapphire resonator exhibits at low temperature extremely low losses, the Fe^{3+} ion concentration required to get enough gain is very low. Contrary to the maser of the 60's, our WhiGMO (Whispering Gallery Maser Oscillator) incorporates a microwave resonator presenting a Q-factor of typically one billion at 4.2K made from a sapphire crystal containing typically 0.1 ppm or less of active ions. The experimental validation of the 12 GHz WhiGMO and its potentiality to be competitive with the state-of-the-art microwave stable references opens the way to revisit the Maser concept and the associated material properties. Moreover the WhiGMO principle can be extended to other transitions of the Fe^{3+} ion in sapphire or to other doped crystals to design stable

*Email: mohamadmrad84@gmail.com

†Email: tarhini.ahmad@gmail.com

‡Email: vincent.giordano@femto-st.fr

sources at higher frequencies.

With this in mind, in the current context, starting from the above introduction, this paper is organized as follows: In section II we introduce the different parts of the molecular hamiltonian, the methods of calculation and the global optimization method based on Shuffled Complex Evolution Model [10]. Then in section III we explain the transition probability between two states using the expression of the dipolar transition moment operator. In section IV we shall explore and discuss the absorbance of a material with related calculations. Then in section V, we show the 31 GHz maser proposal by explaining the corresponding rate equations, signal power and the resonator design. Section VI is devoted to our conclusions.

II. THE MOLECULAR HAMILTONIAN

The Fe^{3+} electronic configuration is [Ar]$3d^5$. The fundamental state spectroscopic term is ^6S (L= 0 and S= 5/2). The Fe^{3+} ion, in a doped sapphire crystal, replaces the Al^{3+} cation and it is subjected to the action of the crystal field of closest ions O^{2-} and Al^{3+} (figure 1). The cation is located in a distorted octahedral. If we assume that the cation Fe^{3+} is in symmetry with O_h, then the fundamental term is $^6A_{1g}(O_h)$.

From the articles of Racah [12], Eliot and Stevens [13] and Judd [14], the interpretation of the theory of an electronic spectra of transition metals became easy. The molecular Hamiltonian is given by:

$$\begin{aligned} H &= H_{ee} + H_{so} + H_c + H_{Zeeman} \\ &+ Trees\ correction + Racah\ correction \end{aligned} \tag{1}$$

We will discuss in this section the energy levels of a transition ion metal in a crystalline solid. The theory is already discussed and determined in detail in [14–18]. The different parts of the hamiltonian are: the electrostatic Coulomb interactions (H_{ee}), the spin-orbit coupling (H_{so}), the ion-ligand interactions described in the case of crystal field theory (H_c), the Zeeman interaction, and the Trees and Racah corrections.

A. Free ion

If we use the method of the "double-zeta exponential", and we assume that the radial function of d orbital can be written as:

$$\begin{aligned} R_d(r) &= a_1(\frac{(2\xi_1)^7}{6!})^{1/2} r^2 exp(-\xi_1 r) \\ &+ a_2(\frac{(2\xi_2)^7}{6!})^{1/2} r^2 exp(-\xi_2 r)\ . \end{aligned} \tag{2}$$

The relation between the previous parameters is:

$$a_1^2 + a_2^2 + 2a_1 a_2 (\frac{2\sqrt{\xi_1 \xi_2}}{\xi_1 + \xi_2})^7 = 1$$

We still have 3 independent parameters (a_1, ξ_1, ξ_2).

From equation (2),the parameters of Racah B_0 and C_0, the spin-orbit coupling constant ζ_0, and the mean values $\langle r^k \rangle_0$ are calculated for the free ion (Zhao [19]).

We don't forget to take the Trees [20] and Racah [21] corrections. The Trees correction constant α_0= 40 cm^{-1} and the Racah correction constant β_0= -131 cm^{-1} are fitted from the spectra of free ion [19].

B. Interaction of crystal field

The crystal field potential can be expressed as a linear combination of irreducible tensor operators C_q^k [16]:

$$H_c = \sum_{kq} B_{kq} C_q^k \tag{3}$$

where B_{kq} are the parameters of crystal field. For d-electrons case, the k integer values can be $0, 2, 4$ and $-k \leq q \leq +k$.

The equation (3) structure is given by the symmetry of the crystal lattice. For a (C_{3v}) trigonal field, the summation has only four terms: B_{20}, B_{40}, B_{43} and B_{4-3}. For the case of a generalized crystal field model, the parameters B_{kq} were given in [11]. The elements of the reduced matrix of tensor operators are given in the book of Nielson and Koster [22] for 16×16 matrices. Using Wigner-Eckart theorem, we develop our generalized model based on 252×252 matrices.

C. Methods of calculation

1. *Optimized parameters*

The interaction term between ligand orbital and central metal ion is complex, so we use an approximation for electrostatic parameters B and C, the spin-orbit constant ζ, the corrections parameters α and β and the average values $\langle r^2 \rangle$ and $\langle r^4 \rangle$:

$$B = N^4 B_0 \quad , \quad C = N^4 C_0 \quad , \quad \zeta = N^2 \zeta_0$$
$$\langle r^2 \rangle = N^2 \langle r^2 \rangle_0 \quad , \quad \langle r^4 \rangle = N^2 \langle r^4 \rangle_0$$
$$\alpha = N^4 \alpha_0 \quad , \quad \beta = N^4 \beta_0$$

where N represents the average reduction factor due to the covalency.
In the Al_2O_3 crystal, the position of Al^{3+} cation is defined respectively to the sites of the two nearest cations as shown in the figure 1.

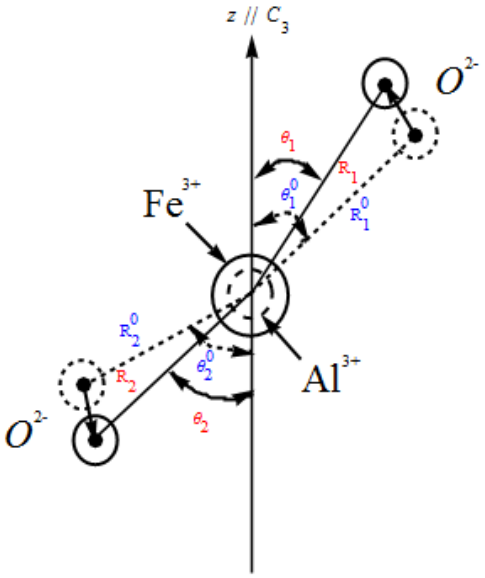

FIG. 1: Local structure distortion of octahedral Fe^{3+} center in α-Al_2O_3 system.

The inter-site distances and the corresponding angles with respect to the axis of symmetry C_3 are given by [23, 24]:

$$R_1^0 = 1.966 \mathring{A} \quad , \quad \theta_1^0 = 47.44^o$$
$$R_2^0 = 1.857 \mathring{A} \quad , \quad \theta_2^0 = 62.70^o$$

Due to the substitution of Al^{3+} by Fe^{3+}, we represent the crystal distortion by assuming, as proposed by Zhao [25], that the two distances is affected by an identical relative variation. We therefore add an identical constraint to the angle relative variations. We then introduce two independent parameters f and g which can be defined as:

$$f = \frac{R_1}{R_1^0} = \frac{R_2}{R_2^0} \quad ; \quad g = \frac{\theta_1}{\theta_1^0} = \frac{\theta_2}{\theta_2^0}$$

Finally the six independent parameters a_1, ξ_1, ξ_2, N, f and g have been modified to approach the experimental observations.

2. Global Optimization Method (GOM)

At Arizona University (SCE-UA), they developed the shuffled complex evolution method [9, 10] which has many advantages. It's a very effective and efficient global optimization method and it can be used to solve problems in non-linear physics with high-parameter dimensions. The aim of this algorithm, developed by Duan in 1992, is to reduce the problem into a best single parameter set in the feasible space. In the current work, this (SCE-UA) method is used to optimize the parameters of the molecular hamiltonian. In other words, it helps to obtain the energy levels (eigenvalues and eigenstates) of the hamiltonian. We want to apply this method in spectroscopy field. We have simplified the problem by using a correlation between different parameters in the previous section. Now, we use a general method: the system has six independent parameters to be optimized.

The optical spectrum of Fe^{3+} in $\alpha - Al_2O_3$ is conveniently represented by choosing:

$$\begin{aligned} a_1 = 0.677\ , \quad \xi_1 = 5.6\ \ , \ \xi_2 = 1.723 \\ N = 0.863\ , \quad g = 0.9958\ \ , \quad f = 1.003 \end{aligned} \tag{4}$$

In Table I, we show the comparison between experimental observations and our calculations. We also compared these results with Zhao's values [11]. We deduce that the introduction of the three free ion parameters and the sixth independent adjustable parameter (g) shows a better results in finding almost all the optical wavelengths in the Fe^{3+} ion spectrum.

To approve our physical description, we derived from our model the spin-Hamiltonian parameters that describe the fundamental state ${}^6A_1(S)$ of the Fe^{3+} ion. Without applying a static magnetic field, there is three energy levels labelled in the following $|i\rangle$ with $i = 1, 2$ or 3 represented in figure 2.

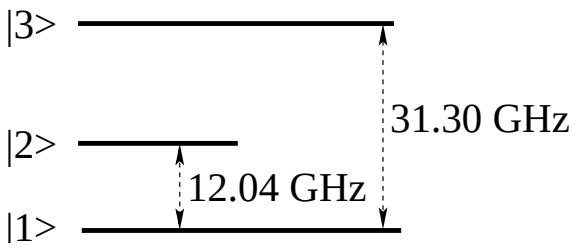

FIG. 2: Structure of Fe^{3+} ground state in the α-Al_2O_3 crystal without applied static magnetic field.

Using the spin hamiltonian expression given in [26], the energy difference between the three hyperfine levels of the ground state are given by:

$$\begin{aligned} E_3 - E_1 &= \frac{1}{3}[(18D + a - F)^2 + 80a^2]^{1/2} \\ E_2 - E_1 &= \frac{3}{2}(a - F) - D + \frac{1}{6}[(18D + a - F)^2 + 80a^2]^{1/2}\ . \end{aligned}$$

The values of the spin hamiltonian calculated parameters: $D, a, a - F$, and the gaps of energy are presented in Table II. They are compared to the Zhao's previous evaluation and the experimental values.

III. PROBABILITY OF TRANSITION

The transition between 2 states i and j, coming from the interaction with an electromagnetic dipole, is proportional to the square of the mean value of dipolar transition moment given as follow:

$$M_{i\to j} = \int \psi^{j*}\hat{\mu}\psi^i d\tau \equiv < \psi^j|\hat{\mu}|\psi^j > \ . \tag{5}$$

TABLE I: Calculation and observation of the d-d transition for the crystal α-$Al_2O_3 : Fe^{3+}$ (Values are in cm^{-1}).

O_h	Zhao [11]	Mrad	Observed [27]
$^4T_1(G)$	9790	9700	9450 - 9700
	10048	9990	
	10229	10128	
	10392	10294	
	10473	10381	
	10493	10396	
$^4T_2(G)$	14229	14183	14350
	14262	14208	
	14315	14219	
	14373	14256	
	14399	14281	
	14401	14282	
$^4A_1(G)$	17977	17875	17600 - 17800
	17998	17897	
$^4E(G)$	18101	18015	
	18143	18056	
	18188	18105	
	18199	18113	
$^4T_2(D)$	20181	20075	
	20191	20078	
	20341	20233	
	20533	20414	
	20562	20432	
	20823	20470	
$^4E(D)$	22299	22195	22120 - 22200
	22313	22212	
	22319	22219	
	22328	22229	
$^4T_1(P)$	25652	25663	25680 - 26700
	25805	25755	
	25945	25875	
	26141	26090	
	26330	26225	
	26457	26526	
$^4A_2(F)$	30167	29884	29000
	30170	29887	

The operator expression of the dipolar transition moment is given by:

$$\hat{\mu} = e\hat{r}.\vec{E} + \beta(\hat{L} + 2\hat{S}).\vec{B} \ . \tag{6}$$

The terms in equation 6 correspond to the electric dipole operator and the magnetic dipole, respectively. In general,

TABLE II: Calculated spin-Hamiltonian parameters for α-$Al_2O_3 : Fe^{3+}$ at 300 K compared to experimental values (the unit is 10^{-4} cm^{-1}).

ZFS parameters	Zhao[11]	Mrad	Observed[28, 29]
D	1784	1723	1718 ± 2
a-F	322	330	329 ± 2
a	254	268	241 ± 4
$E_3 - E_1$	10838	10478	10451
$E_2 - E_1$	4118	4011	4015

the interaction between electric dipole with the light electric field dominates the transition by 4 orders of magnitude the interaction of magnetic dipole with magnetic field.

The optical spectrum of the iron doped sapphire shows a quite intense absorption bands [27, 30]. Thus it indicates the possibility of optical interaction with the Fe^{3+} ions. Our goal is to show the possibility to get a population inversion in the ground state by applying an optical radiation to the crystal. Thus we need to calculate the effect of an optical radiation on the population of each ground state level $|i\rangle$, with $i = 1, 2$ or 3. We have to take into consideration that the allowed transitions with different excited levels $|j\rangle$ are listed in the table I. The transition rate W_{ij} between one ground state level $|i\rangle$ and one excited level $|j\rangle$ is given by (Siegman [1]):

$$W_{ij} = W = \frac{1}{4}(\gamma \mathrm{H})^2 g(\nu)\sigma^2 \tag{7}$$

where γ is the gyromagnetic factor, H is the module of the RF or the optical magnetic field and $g(\nu)$ is the line shape function describing the spectral broadening of the absorption line.

The dimensionless factor σ^2 represents the strength of the probability of transition. It depends on the relative orientation of the oscillating magnetic field with respect to the crystal axis z. σ^2 is computed from the matrix element of the interaction hamiltonian, which depends on the total magnetic momentum and the applied oscillating magnetic field. In our case, two different orientations have to be considered since we don't have a static magnetic field: H $\perp z$ or H$//z$. We found that, for each transition, only one configuration gives noticeable value for σ^2. In Table III, we give the relevant σ^2_{ij} parameters for each transition. The relative orientation of H with respect to z is indicated by the symbol ($\perp$) or ($//$).

IV. ABSORBANCE

In spectroscopy domain, the absorbance (also called optical density) of a material is a logarithmic ratio between the falling and transmitted radiation through this material. Thus,

$$A = \lg(P_0/P_{trans}) \tag{8}$$

where P_0 is the power of the incident radiation and P_{trans} is the intensity of the transmitted radiation from the material. So we can decompose P_0 into two parts:

$$P_0 = P_{abs} + P_{trans}$$

where P_{abs} is the total power absorbed by the ions. The power per unit volume can be written as:

$$\mathrm{d}P_{abs} = h\nu W \Delta n \mathrm{d}V$$

From equation 7, the transition rate is proportional to the square of the transverse magnetic field. According to the Pointing vector, this rate is proportional to the power of the applied wave (This is done in the Appendix A of Mrad's thesis [38]).

After an integral calculation, the relation between absorbed and transmitted powers in a waveguide of length L can be expressed as:

$$P_{abs}(L) = P_0(1 - e^{-\alpha L}) = P_0 - P_{trans} \tag{9}$$

TABLE III: Strength of transition probability σ^2 for the Fe^{3+} d-d transitions in $\alpha - Al_2O_3$. The integer (n) in brackets is for $\times 10^{-n}$).

O_h	σ^2_{1j}	σ^2_{2j}	σ^2_{3j}
$^6A_1(S)$	2.00 (0) [$\perp$]	-	-
	3.27 (3) [$\perp$]	1.25 (0) [$\perp$]	-
$^4T_1(G)$	1.84 (6) [//]	7.43 (5) [$\perp$]	1.70 (6) [$\perp$]
	1.52 (5) [$\perp$]	2.85 (6) [//]	9.63 (5) [$\perp$]
	8.53 (7) [$\perp$]	1.88 (5) [$\perp$]	1.33 (4) [//]
	2.17 (5) [$\perp$]	9.90 (5) [//]	6.19 (6) [$\perp$]
	4.08 (5) [//]	4.34 (6) [$\perp$]	4.63 (7) [$\perp$]
	1.95 (5) [//]	8.90 (6) [$\perp$]	3.64 (7) [$\perp$]
$^4T_2(G)$	6.87 (4) [//]	2.08 (4) [$\perp$]	2.74 (4) [$\perp$]
	5.92 (5) [//]	1.37 (7) [$\perp$]	4.70 (4) [$\perp$]
	5.35 (6) [$\perp$]	2.21 (4) [//]	1.61 (4) [$\perp$]
	2.97 (5) [$\perp$]	5.56 (4) [$\perp$]	1.43 (4) [//]
	1.71 (4) [$\perp$]	5.12 (10) [$\perp$]	4.06 (4) [//]
	1.73 (4) [$\perp$]	4.65 (4) [//]	1.36 (5) [$\perp$]
$^4A_1(G)$	3.43 (3) [//]	1.41 (4) [$\perp$]	4.29 (4) [$\perp$]
	7.01 (4) [$\perp$]	3.24 (5) [//]	1.05 (3) [$\perp$]
$^4E(G)$	**1.40 (3)** [$\perp$]	**1.80 (4)** [$\perp$]	**8.32 (4)** [//]
	1.29 (4) [$\perp$]	1.16 (3) [$\perp$]	1.83 (3) [//]
	8.88 (4) [//]	1.70 (3) [$\perp$]	6.70 (4) [$\perp$]
	2.67 (5) [$\perp$]	4.62 (3) [//]	1.26 (3) [$\perp$]
$^4T_2(D)$	5.55 (5) [//]	2.23 (5) [$\perp$]	2.90 (5) [$\perp$]
	6.96 (6) [$\perp$]	7.68 (6) [//]	5.84 (5) [$\perp$]
	4.50 (5) [$\perp$]	4.93 (5) [$\perp$]	1.62 (4) [//]
	1.39 (6) [//]	8.22 (6) [$\perp$]	1.01 (5) [$\perp$]
	7.80 (5) [$\perp$]	2.42 (4) [//]	2.90 (5) [$\perp$]
	4.73 (5) [//]	9.33 (7) [$\perp$]	8.77 (5) [$\perp$]
$^4E(D)$	9.67 (8) [//]	2.80 (7) [$\perp$]	2.31 (8) [$\perp$]
	9.12 (9) [$\perp$]	5.53 (7) [$\perp$]	7.05 (7) [//]
	2.29 (7) [$\perp$]	1.11 (7) [//]	1.80 (7) [$\perp$]
	2.23 (8) [$\perp$]	7.54 (8) [$\perp$]	4.09 (7) [//]
$^4T_1(P)$	1.27 (5) [//]	1.71 (7) [$\perp$]	6.22 (7) [$\perp$]
	4.15 (6) [//]	5.79 (7) [$\perp$]	2.58 (8) [$\perp$]
	3.14 (5) [//]	1.31 (5) [$\perp$]	8.33 (7) [$\perp$]
	4.22 (9) [$\perp$]	6.69 (6) [//]	4.27 (5) [$\perp$]
	2.35 (6) [//]	2.19 (5) [$\perp$]	5.23 (8) [$\perp$]
	9.36 (7) [//]	1.61 (7) [$\perp$]	1.59 (8) [$\perp$]
$^4A_2(F)$	2.10 (8) [$\perp$]	6.58 (7) [//]	2.63 (7) [$\perp$]
	1.20 (7) [//]	6.33 (11) [$\perp$]	2.90 (7) [$\perp$]

where α is the absorption coefficient, its expression is given as:

$$\alpha = \frac{h\gamma^2 g(\nu)\Delta n}{2Z_T}\nu\sigma^2$$

where Z_T represents the characteristic impedance of the guide. We put equation 9 in equation 8 in order to obtain the absorbance A:

$$A = \alpha L$$

At the end, we conclude that A is proportional to the product $\nu\sigma^2$, so to $\bar{\nu}\sigma^2$. In the figure 3, we plot the absorbance and the product $\bar{\nu}\sigma^2$ versus wavenumber $\bar{\nu}$ (unit cm^{-1}).

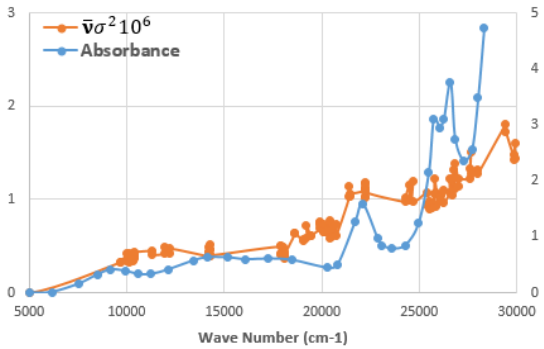

FIG. 3: Comparison between experimental absorbance [27] and the product $\bar{\nu}\sigma^2$ versus wavenumber $\bar{\nu}$

V. 31 GHZ MASER PROPOSAL

Laser sources emitting some 100 mW at 555 nm, with a linewidth less than 0.1 nm, are currently commercially available (see for example [31]). We select from the table III, the transition to the $^4E(G)$ excited level, at $18015cm^{-1}$ ($\approx$ 555 nm). The transition probabilities for the $^6A_1(S) \longrightarrow {}^4E(G)$ transition with H $\perp z$ are: $\sigma_1^2 = 1.40\times10^{-3}$, $\sigma_2^2 = 1.80\times10^{-4}$ and $\sigma_3^2 \approx 0$. So if we submit the crystal to a narrow band 555 nm laser source, the $|1\rangle$ level will be more effectively pumped. Therefore we can obtain large population differences between $|1\rangle$ and the two other ground state levels.

A. Rate equations

If we consider a Fe^{3+} doped Al_2O_3 crystal submitted to a 555 nm narrow band source resonant with the transition $^6A_1(S) \longrightarrow {}^4E(G)$. The proposed system is schematized in figure 4. A cylindrical cryogenic sapphire resonator presenting a high-Q resonance mode at 31 GHz is submitted to an optical radiation at 555 nm. The crystal axis z is collinear to the cylinder axis. The 31 GHz resonant mode is assumed to be quasi-transverse magnetic, i.e. the magnetic field lines, in the equatorial plane of the cylinder, are perpendicular to the z axis. A small magnetic loop placed near the dielectric cylinder is used to derive the 31 GHz maser signal output.

The excited levels decay quickly to the ground state with a lifetime $\tau_0 \ll 1$ ms. All relaxation in the ground state are governed by the spin-lattice effect with a characteristic time $\tau_1 \approx 10$ ms at 4 K. It is also determined that the spin-to-spin relaxation is very fast with a characteristic time $\tau_2 \leq 20$ ns. If we neglect coherence and we deal only with level populations, so a model with a simple rate equations is sufficient to describe the interaction [32]. There is a possibility that the excited ions may fall on intermediate levels, but since $\tau_0 \ll \tau_1$ they relax rapidly to ground state. This fact leads to consider only a four levels system: the three ground state levels and the $^4E(G)$ excited one, which is labelled $|4\rangle$. The absorption rate W_P due to excitation of the ground state ions from the optical radiation is evaluated using equation 7. The optical pumping gives the possibility to get a population inversion between $|3\rangle$ and $|1\rangle$. Therefore one can obtain a maser effect at 31 GHz provided that the resonator has been designed to exhibit a high Q resonance at this frequency.

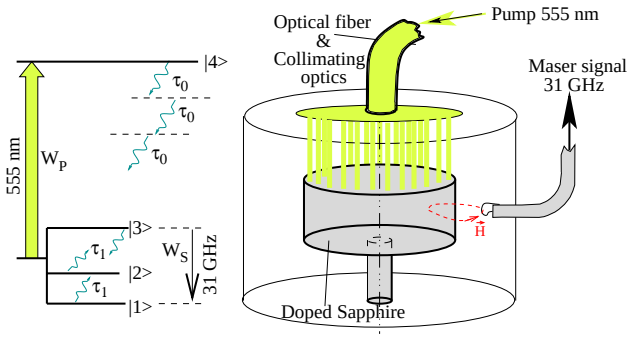

FIG. 4: Energy levels and schematic of the cryogenic optically pumped 31 GHz WhiGMO.

The first 31 GHz emitted photons will stimulate others emissions with a rate W_S. If the optical pumping is efficient enough to compensate for the loss of the resonator,a self-sustaining 31 GHz oscillation will occur. We have followed the method described in [33] (validated in case of 12 GHz WhiGMO), in order to determine theoretically the conditions to get a 31 GHz maser signal. The stationary solutions of the rate equations are:

$$\Delta n_{13} = \frac{27\Delta N_{13} + 6(2\Delta N_{13} - 3\Delta N_{14})\tau_1 W_P}{9(3 + 4\tau_1 W_S) + 4(3 + \tau_1 W_S)\tau_1 W_P} \tag{10a}$$

$$\Delta n_{14} = \frac{9(3\Delta N_{14} + 2(2\Delta N_{14} - \Delta N_{13})\tau_1 W_S)}{9(3 + 4\tau_1 W_S) + 4(3 + \tau_1 W_S)\tau_1 W_P} \ , \tag{10b}$$

where ΔN_{ij} and Δn_{ij} are the difference in population between two levels $|i\rangle$ and $|j\rangle$ at the thermal equilibrium and in the presence of the pump and maser signal, respectively. ν_{14} and ν_{13} represent the frequencies of the pump and the maser signal respectively.

B. Threshold pump power

When the population inversion takes place, the threshold pump power is achieved in the absence of the maser signal. By taking Δn_{13}= 0 in equation (10a), we can find the absorption rate W_{P_0} corresponding to this situation:

$$W_{P_0} = \frac{9}{2\tau_1} \frac{\Delta N_{13}}{3\Delta N_{14} - 2\Delta N_{13}} \tag{11}$$

The total absorbed power can be written as:

$$\begin{aligned} P_0 &= h\nu_{14} W_{P_0} \Delta n_{14_0} N V_{eff} \\ &= \frac{3}{2\tau_1} h\nu_{14} \Delta N_{13} N V_{eff} \end{aligned} \tag{12}$$

where N is the concentration of Fe^{3+} ions, and V_{eff} is the volume occupied by the active ions which participate to the maser signal. V_{eff} is the volume of the 31 GHz mode in the sapphire resonator (see section V D). Here, we assume that the optical radiation only illuminates the resonator part where the 31 GHz mode is concentrated. P_0 is thus the minimal optical power required to get maser action in optimized conditions.

C. Maximum maser signal power

Δn_{13}, and thus the 31 GHz maser signal power, increase with the pump signal power system until the saturation of the optical transition occurs, i.e $n_4 \simeq n_1$. Assuming we already overcome this situation, i.e. $W_P \to \infty$, equations (10a-10b) will simplify and the maximum maser power is calculated to obtain:

$$\begin{aligned} P_{31_{max}} &= h\nu_{13} \ Max[W_S \Delta n_{13}] N V_{eff} \\ &= \frac{3}{2\tau_1} h\nu_{13} (3\Delta N_{14} - 2\Delta N_{13}) N V_{eff} \end{aligned} \tag{13}$$

$P_{31_{max}}$ is the total power generated by the active ions inside the resonator. The coupling loop derive only a fraction of this power depending on the coupling coefficient β, which is related to the loop area and to its position with respect to the sapphire resonator. For a critical coupling , i.e. $\beta = 1$, the maser output power is one half of $P_{31_{max}}$. The resonator Q-factor is also impacted by the loading to the external circuit. For $\beta = 1$, the loaded Q-factor is one half of the unloaded one.

D. Resonator design

Our objective is to use the Fe^{3+} ions present as contaminant in a high purity sapphire monocrystal. Typical effective ions concentration in such a type of crystal is well below 1 ppm. Thus the 31 GHz resonator has to present a very high quality factor, otherwise the 31 GHz stimulated emissions will not be sufficient to compensate for the resonator loss. This can be accomplished by using a whispering gallery mode, which Q-factor is only limited by the sapphire losses. Quasi–TM Whispering gallery modes are characterized by three integers m, n, l which represent the electromagnetic field component variations along the azimuthal, radial and axial directions respectively [34]. In the following we consider only the resonant modes with low radial and axial variations, i.e. those corresponding to $n = l = 0$. At low temperature, i.e. near the liquid helium temperature, the whispering gallery mode Q-factor can be as high as 1 billion providing the mode order is sufficiently high, i.e. $m > 15$ [35]. The WhiGMO principle has been demonstrated at 12 GHz, i.e. the frequency of the $|1\rangle \rightarrow |2\rangle$ transition. In this case, the population inversion results from a pumping at 31 GHz. The resonator has a diameter $2R = 50$ mm and a thickness $h = 30$ mm. The quasi-TM Whispering Gallery mode $WGH_{17,0,0}$ is used to support the maser signal [36].

For the whispering gallery mode the electromagnetic fields are concentrated near curved air-dielectric interface, between the resonator radius R and a caustic of radius R_C. The effective volume $V_{eff} = \pi h \left(R^2 - R_C^2\right)$ occupied by the mode is a little mode dependant as R_C is given by:

$$R_C = \frac{m}{\sqrt{\epsilon_r \left(\frac{\nu_{13}}{c}\right)^2 - \left(\frac{\pi}{2h}\right)^2}} \tag{14}$$

where $\epsilon_r \approx 9.4$ is the sapphire permittivity is the transverse direction with respect z. c the velocity of light in vacuum.

To design a 31 GHz resonator we keep the same ratio diameter/thickness, which is near the optimal value [37]. Thus to design the cryogenic resonator only means choosing the azimuthal number for the mode supporting the 31 GHz signal. m has to be higher than 15 to prevent radiation losses which limit the Q-factor and should not be to high otherwise the coupling with the output probe will be difficult to adjust. The table IV gives for different values of m, the resonator diameter $2R$, the threshold optical power P_0 and the maximum maser power emitted by the ions. Here, the Fe^{3+} concentration is assumed to be 0.02 ppm, i.e. the same value than the 12 GHz WhiGMO.

TABLE IV: Different resonator designs to support the 31 GHz signal. The pump threshold power P_0 and the maximum maser power $P_{31_{max}}$ are given for few azimuthal numbers as well as the resonator diameter assuming a constant ratio $\frac{2R}{h} = \frac{5}{3}$.

m	$2R$ (mm)	P_0 (mW)	$P_{31_{max}}$ (μW)
17	19.22	1.17	1.02
19	21.13	1.42	1.24
21	23.05	1.71	1.49
25	26.88	2.35	2.05
35	36.46	4.40	3.85
49	50.00	8.41	7.36

VI. CONCLUSION

In this work we refined the description of the Fe^{3+} ion embedded into a (α-Al_2O_3) matrix to derive its 252 energy levels with two optimization methods "local and global", whose the global method is based on Shuffled Complex Evolution Model. Moreover we calculated the Fe^{3+} ion strength transition probability including those for optical transitions. It appears than a few allowed optical transitions are favorable to obtain a maser operation at 31 GHz applying optical pumping at wavelength achievable with available low cost laser sources. Eventually, a first preliminary evaluation of the 31 GHz maser concept is presented. We have also shown that the 31 GHz maser signal power achievable is larger than the classical 12 GHz version, i.e. a power gain of 100 is expected in the optimized conditions. As fundamental limit of frequency stability is fixed by the thermal noise, any increase in the maser signal output will benefit to the performance.

[1] A. E. Siegman, Microwave Solid State Masers, New York : McGraw-Hill (1964).
[2] J.P. Gayga and J. Hervé, Revue de Physique Applique, **6**, p. 177-179, (1971).
[3] D.P. Devor, I.J. D'Haenens and C.K. Asawa, Phys. Review Letters, **8**, 11, p. 432-435, (1962).
[4] P. Y. Bourgeois, N. Bazin, Y. Kersalé, V. Giordano, M. E. Tobar, and M. Oxborrow, Applied Physics Letters 87(22), 224104-1-3 (2005).
[5] Benmessai K., Bourgeois P.Y., Kersalé Y., Bazin N., Tobar M.E., Hartnett J G, Oxborrow M, and Giordano V., Electron. Lett., 43, 1436, (2007).
[6] V. Giordano, S. Grop, B. Dubois, P.-Y. Bourgeois, Y. Kersalé, G. Cabodevila, E. Rubiola, and G. Haye, Proc. of the 3rd International Colloquium - Scientific and Fundamental Aspects of the Galileo Programme, 31 August - 2 September (2011), Copenhagen, Denmark.
[7] T. Kessler, C. Hagemann, T. Legero, U. Sterr, F. Riehle, M. Martin and J. Ye. Proc. of the 2011 Joint Conf. of the IEEE International Frequency Control Symposium and The European Frequency and Time Forum, May 1-5, p. 699-700, (2011) San Fransisco, California, USA.
[8] M. J. Thorpe, L. Rippe, T. M. Fortier, M. S. Kirchner and T. Rosenband, Nature Photonics, 5, 688-693, (2011).
[9] Duan, Q., V. K. Gupta, and S. Sorooshian, Water Resources Research, 28, 1015-1031, (1992).
[10] Duan, Q., V. K. Gupta, and S. Sorooshian, Journal of Optimization Theory and Applications, 76(3), 501-521, (1993).
[11] M. G. Zhao and M. Chui, Phys. Rev. B 52 (1995).
[12] G. Racah, Phys. Rev. 62, 438 (1942); 63, 367 (1943); 76, 1352 (1949); 85, 381 (1952).
[13] R. J. Elliot and K. W. H. Stevens, Proc. Roy. Soc. A218, 553 (1953); A219, 387 (1953); A65, 209 (1963).
[14] B. J. Judd, Second Quantization and Atomic Spectroscopy, John Hopkins University Press (1967).
[15] B. R. Judd, Operator techniques in atomic spectroscopy (1963).
[16] B. G. Wybourne, Spectroscopic properties of rare earths (1965).
[17] A. Abragam and B. Bleaney, Electron paramagnetic resonance of transition ions (1986).
[18] G. Liu and B. Jacquier, Spectroscopic properties of rare earths in optical materials (2005).
[19] M. G. Zhao and M. Chui, Phys. Rev. B 49, 12556 (1994).
[20] R. E. Trees, Phys. Rev. 85, 6 (1951); Phys. Rev., 83-4 (1951); Phys. Rev., 123-4 (1961)
[21] G. Racah, Phys. Rev. 83, 4 (1951).
[22] C. W. Nielson and G. F. Koster, Spectroscopic Coefficients for the p^n, d^n and f^n Configurations Cambridge, Massachusetts (1963).
[23] D. S. MacClure, J. Chem. Phys. 38, 2289 (1963).
[24] K. Moorjani, N. Moorjani, and N. Meavoy, Phys. Rev. 132, 504 (1963).
[25] M. G. Zhao, Chemical-Physics 18, 109 (1998).
[26] B. Bleaney and al., Reports on Progress in Physics (1953).
[27] G. Lemann and H. Harder, Am. min. 55, 98 (1970).
[28] G. S. Bogle and H. F. Symmons, Proc. Phys. Soc. 73, 531 (1959).
[29] S. Lee, C. M. Brodbeck and C. Yang, Phys. Rev. B 15, 2469 (1977).
[30] G. Lemann, Am. min. 56 (1971).
[31] www.crystalaser.com.
[32] M. Mrad, P.-Y. Bourgeois, M.E. Tobar, Y. Kersalé, V. Giordano, Eur. Phys. J. Appl. Phys., 57, 21005 (2012).
[33] K. Benmessai, P. Y. Bourgeois, M. E. Tobar,N. Bazin,Y. Kersalé, and V. Giordano, Meas. Sci. Technol., 21, 025902 (2010).
[34] X.H. Jiao, P. Guillon, L.A. Bermudez, IEE Proc., 154, 497-501 (1987).
[35] P.Y. Bourgeois, Y. Kersalé, N. Bazin, M. Chaubet, and V. Giordano, IEEE Trans. on UFFC, 51(10), 1232-1239, (2004).
[36] P.-Y. Bourgeois, M. Oxborrow, M. E. Tobar, N. Bazin, Y. Kersalé and V. Giordano. Int. J. of Modern Physics B, 20, n 11-12 & 13, 1606-1612, (2006).
[37] J. Krupka. D. Cros, A. Luiten and M. Tobar, Electronics Letters, 32(7), 670-671, (1996).
[38] M. Mrad, Effets Maser et CPT des ions paramagnétiques, Ph.D. thesis, Université de Franche-Comté (2012).